Indian Journal of Geo Marine Sciences
Vol. 54 (08), August 2025, pp. 398-413
DOI: 10.56042/ijms.v54i08.14451

Research Article

Geochemical and petrographic characterisation of serpentinised peridotite from the Indian Ocean: Insights into mantle processes and tectonic evolution

M Pilgaonkar*[,a], P D Sawant[a] & R Mukhopadhyay[b]

[a]School of Earth, Ocean and Atmospheric Sciences, Goa University, Taleigao Plateau, Goa – 403 206, India

[b]CSIR-National Institute of Oceanography, Dona-Paula, Goa – 403 004, India

*[E-mail: mrunalipilgaonkarwork29@gmail.com]

Received 17 October 2024; revised 13 July 2025

The present study explores the intriguing serpentinised peridotites from the Central Indian Ridge, discovered during the Sagar Kanya SK-195 cruise (2003). Detailed petrographic analysis revealed high-relief olivine and clinopyroxene, with orthopyroxene showing high-temperature deformation, along with opaque Cr-spinel and magnetite minerals. Mesh and brucite textures are prominent. Degree of serpentinisation was confirmed by the presence of antigorite, lizardite, and chrysotile, observed using Electron Microprobe Analysis EPMA and BSE imaging. Geochemical data indicated a harzburgitic protolith with iron-rich lizardite, and significant Fe enrichment in chromiferous spinel. Spinel, a quantitative melting indicator of mantle residues, exhibits compositional diversity and relative proportions of Cr, Fe, and Al in spinel-group minerals. REE patterns showed a distinct U-shape with a positive Eu anomaly, suggesting the absence of plagioclase feldspar. Major element analyses, supported by MgO/SiO_2 *vs*. Al_2O_3/SiO_2 trends, indicated 25 – 30% of partial melting, and a negative magnesium loss trend was also observed. Abyssal peridotite samples revealed the effect of regional geological processes and environments. Spinel Cr# and Mg# ratios and variations in Th, Zr, and Nb concentrations reflected complex melt-rock interactions. Characteristics of serpentinised peridotites suggest a heterogeneous origin influenced by multiple tectonic episodes and shared source material, enhancing understanding of serpentinisation, mantle melting, and the geochemical evolution of oceanic peridotites.

[**Keywords**: Central Indian ridge, Chromiferous spinel, Degree of serpentinisation, Harzburgitic protolith, Melt rock interaction, Partial melting]

Introduction

Mantle peridotites are extensively exposed on the seafloor at slow-to-intermediate spreading ridges, serving as residues from variable degrees of partial melting linked to mid-ocean ridge basalt production[1-12]. It reveals the nature of the deeper sub-ocean lithosphere and asthenosphere, and is prevalent in slow-spreading ridges, often representing hydrated mantle diapirs uplifted near transform faults[13]. The formation of serpentinites from peridotites is key to understanding low-temperature metamorphism[14]. Abyssal peridotites, exposed through tectonic faulting at slow and ultraslow spreading ridges, are integral to hydrothermal interaction processes at divergent plate margins[15-18]. Despite serpentinisation, relics of mantle minerals in abyssal peridotites retain critical information on melting and melt extraction beneath mid-ocean ridges, highlighting the importance of hydrothermal interaction in the rheology of the oceanic lithosphere[19-23], geochemical budgets[24-26], and microbial activities[27-29].

Exposures of serpentinites are notably frequent along the Mid-Atlantic Ridge (MAR), Southwest Indian Ridge (SWIR), and Gakkel Ridge, with various studies documenting occurrences through dredging or drilling at MAR's axial valleys, transform faults, and detachment faults[26,30-37]. Similar findings have been reported from the East Pacific Rise (EPR) and the Galapagos Spreading Centre[38], with less frequent reports from the Carlsberg-Central Indian Ridges (CR-CIR)[39,40].

Detailed mineralogical, chemical, and petrographic studies remain sparse for many sites, especially in the Indian Ocean Ridge System (IOR)[41-43]. Studies on spinel chemistry have focused on various ridges, including MAR, Hess Deep, EPR, SWIR, and Gakkel Ridge[8,37,43-48]. Spinel composition, particularly chromium spinel-bearing peridotites, is a crucial tracer of mantle melting processes[8,44,49].

While petrological studies of the Northern Central Indian Ridge (NCIR) have concentrated on basalt geochemistry and magmatic processes[50-56], detailed investigations into mantle peridotite and serpentinite

geochemistry are limited[41,57]. Recent studies have begun to address the degree of partial melting and element behaviour during serpentinisation in the southern CIR[8,29], leaving the NCIR less explored. Hydrothermal systems along these ridges exhibit significant CH_4 and Mn anomalies, indicative of peridotite-hosted systems[58-60].

This study presents a new report on the petrography, mineral chemistry, and whole-rock chemistry of serpentinite peridotite recovered from a depth of 2700 m at latitude 06°38'30.36" S, and longitude 68°19'20.40" E, located between the Vityaz and Vema Fracture Zones on the Central Indian Ridge (Fig. 1). These samples were collected in 2003 during the Sagar Kanya SK-195 cruise (DR#9) conducted by the National Institute of Oceanography, Dona Paula, Goa. This study aims to elucidate the geochemical systematics of abyssal peridotites to understand the impact of hydrothermal alteration on their composition, thereby contributing to the characterisation of the geochemical budget of the lithosphere at slow and ultraslow-spreading ridges.

Geological setting

The Indian Ocean includes five significant mid-ocean ridge systems: the Carlsberg Ridge (CR), North Central Indian Ridge (NCIR), South Central Indian Ridge (SCIR), Southeast Indian Ridge (SEIR), and Southwest Indian Ridge (SWIR). The mid-ocean ridges are characterised by divergent plate boundaries, where tectonic plates separate, allowing magma to rise and form new, fresh oceanic crust.

This geological activity contributes to the region's ecological and geological diversity, influencing the geochemistry of the ocean floor. Basalt and gabbro are prevalent rock types present along the CIR (along both NCIR and SCIR). Basalt, formed by the rapid cooling of lava derived from the mantle, is a finely-grained, dark-coloured volcanic rock. Gabbro is a coarse-grained intrusive igneous rock that results from the crystallisation of mantle magma beneath the Earth's surface[15,37].

The Central Indian Ridge (CIR), a slow-to-intermediate-spreading ridge, is crucial in separating the African Plate from the Indo-Australian Plate.

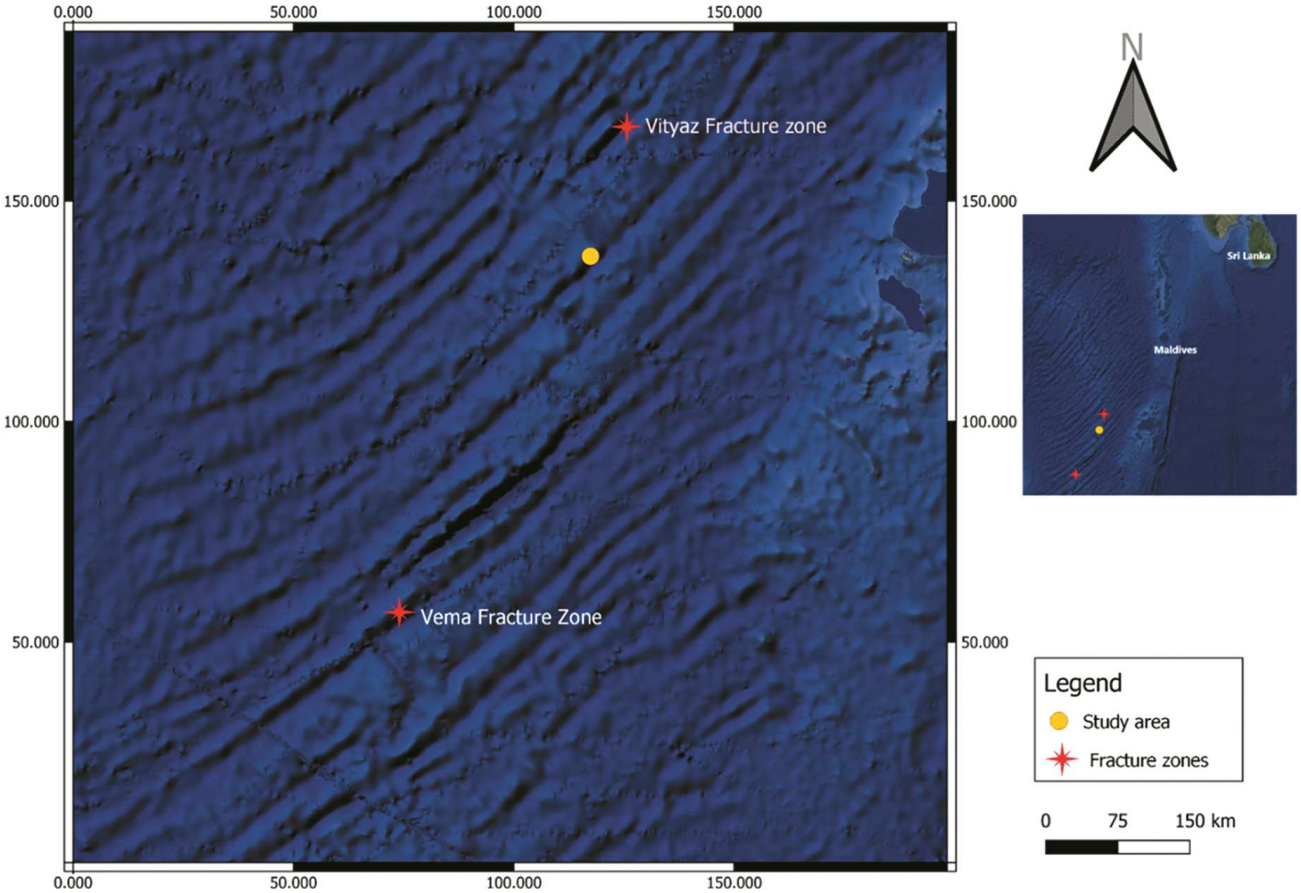

Fig. 1 — Location map of the study area situated on CIR and between Vityaz and Vema fracture zone

It features a 500–1000 m deep axial valley, with 50–100 km-long ridge segments interrupted by transform faults and non-transform discontinuities. The ridge is characterised by axial volcanic ridges that are 15 km long, 1–2 km wide, and rise 100–200 m above the axial floor, indicative of melt supply from the Earth's mantle forming new oceanic crust[16].

The Central Indian Ridge (CIR) demonstrates an intermediate spreading rate of about 30 mm/yr close to the Equator and 49 mm/yr near the Rodrigues Triple Junction (RTJ). The ridge displays moderate obliquity with few large offsets, except for notable features like the Mary Celeste Fracture Zone at 18° S. The SCIR maintains near-orthogonality, whereas the NCIR trends North North-West (NNW) and lacks fracture zones. The axial depth of the CIR varies, increasing from 3200 m at 20° S to 4000 m at the RTJ[(ref. 18)].

Dredge samples weighing approximately 1200 kg were recovered from a depth of 2700 m. The samples comprised serpentinite, serpentinite basalt, gabbro, and calcareous sediments, displaying variations in size, distinct striations, and slickenside structures.

Materials and Methods

From the recovered dredged material, twelve representative serpentinised peridotite samples were selected. Thin sections were meticulously prepared for petrographic study. A Nikon Eclipse E200 polarising microscope was used, while powdered samples were utilised for geochemical analysis using XRF and ICP-MS for major element analysis. The process for detailed petrography entailed cutting and grinding thin sections to 2–4 mm thickness, ensuring parallelism by sanding and subsequent grinding until smooth. Polishing was achieved using diamond polishing powder and slow-set epoxy for optimal bonding with glass, resulting in near-transparency.

Mineral compositions were estimated by Electron Probe Micro Analyses (EPMA) on well-polished thin sections coated with a carbon film for uniform electrical conductivity. Quantitative chemical analyses were carried out at the National Institute of Oceanography (NIO) in Goa using Wavelength Dispersive Spectrometry (WDS) on a CAMECA X5 electron probe micro analyser, following established nomenclatorial rules for mineral classification.

Major element concentrations in 12 serpentinised peridotite samples were determined at NIO (Goa) using X-ray Fluorescence spectrometry (XRF) with a spectrometer operating in sequence mode. Samples were prepared into 32 mm beads using Merck's Spectromelt A12 and a powdered sample, followed by heating and cooling to create glass beads for analysis using a PANalytical Axios spectrometer based on standards BHVO-2 and BCR-2.

Trace and REE compositions were analysed at CSIR-National Geophysical Research Institute (NGRI), Hyderabad, using a closed digestion method with HF:HNO_3 acids for sample digestion. An internal standard of 1 ppm Rhodium was added for analysis using a High-Resolution Inductively Coupled Mass Spectrometer (HR-ICP-MS) in jump-wiggle mode at CSIR-NGRI, Hyderabad. Certified reference materials UBN were utilised to ensure accuracy, and data processing was performed using NuQuant® software for automated/manual interpretation of spectra.

Results

Petrographic observations

This study delves into the petrographic intricacies of serpentinised peridotite, a metamorphic process involving the hydration of olivine and pyroxene in Earth's lithosphere. Aimed to enhance understanding of the evolution of serpentinised peridotite and its geological significance, a NIKON ECLIPSE E200 polarising microscope was used. Peridotite, comprising olivine and clinopyroxene and classified as lherzolite, exhibits high relief and limited colour distinction, posing challenges in pyroxene identification. Olivine grains exhibit higher relief and brighter interference colours in crossed polars, with distinct grain boundaries indicating minor alteration likely due to serpentinisation. Orthopyroxene (Fig. 2a) displays cleavage, first-order grey interference colours, elongation suggestive of high-temperature deformation, and opaque Cr-spinel minerals[48,61,80].

The captivating process of serpentinisation involves the metamorphosis of olivine into serpentine, a hydrated magnesium silicate mineral with a low birefringence and a mesh-like texture. Serpentinites often retain olivine and pyroxene remnants, displaying high relief and low birefringence. Antigorite (Fig. 2c), a serpentine type, has a consistent fine-grained cross-hatched texture, while serpentinite forms fine laths with low relief and low interference colours[48,61,80]. In peridotite rock, bastite

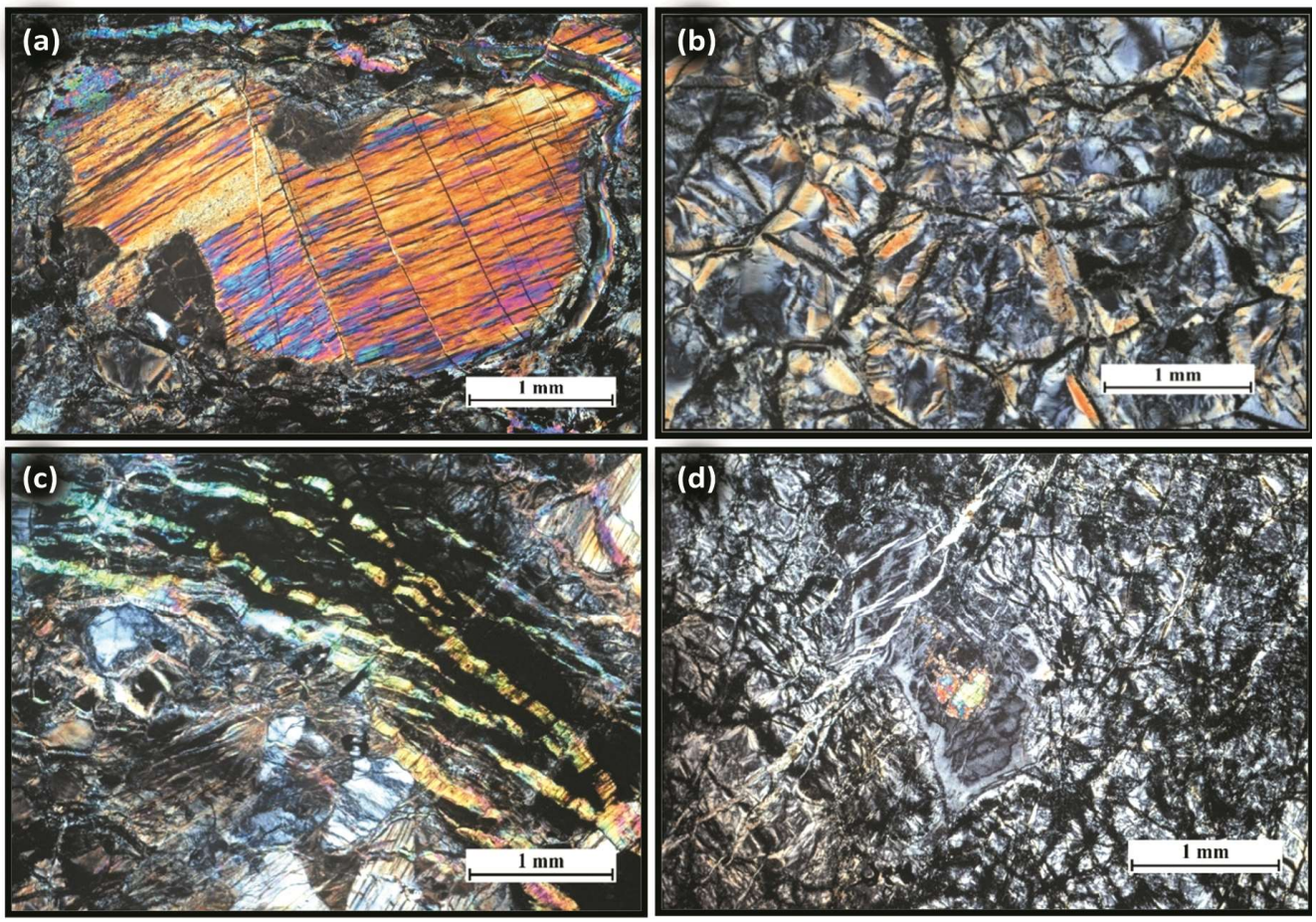

Fig. 2 — a) Diopside crystals embedded in mesh texture; b) Olivine altered to serpentine mineral, mesh texture; c) Antigorite polymorph of serpentine; and d) Brucite texture observed in pyroxene[48,61,80]

crystals tend to interconnect with other serpentine minerals and with each other, creating a cohesive network. Bastite typically exhibits a brownish tint due to impurities. Over time, the original olivine crystals in the peridotite are replaced by bastite, resulting in pseudomorphic textures where the original form of olivine is preserved. However, its mineral composition has changed to bastite.

The structure and content of the serpentinised peridotite are influenced by the presence of bastite[48,61,80] (Fig. 2d) along with other secondary minerals such as brucite, magnetite, and chromite. These minerals form during serpentinisation. Augite, a common pyroxene in basic and intermediate igneous rocks, shows moderate to high relief, fractures, and a mesh texture (Fig. 2b) with pink second-order interference colours[48,61,80]. Orthopyroxene crystals are pink or greenish, displaying pleochroism, cleavage, and fractures. Talc and tremolite exhibit distinctive characteristics indicative of their formation processes during alteration and metamorphism.

Mineral chemistry

The study investigates the mineral chemistry of serpentinised peridotites (Table S3), focusing on the detailed characterisation of their mineralogical composition. Stoichiometry for each mineral crystal (Tables S1, S2, S3) was calculated and normalised to the number of oxygen atoms in the chemical formula, with end-member compositions expressed as molar percentages. To distinguish different mineral zones within the sample, Backscattered Electron (BSE) imaging was utilised, capitalising on the contrast variations arising from differences in atomic number. These variations, effectively highlight changes in mineral composition, providing a valuable guide for the analysis.

In a previous discussion[61] the chemical composition of serpentine minerals, including chrysotile, lizardite, and antigorite was examined (Table S3). Antigorite, the most common serpentine mineral, has a well-studied composition with a higher magnesium concentration than iron. Lizardite, another

type of serpentine, has a higher iron concentration and is often found in hydrothermal veins and low-grade metamorphic rocks. The majority of samples in the study were found to have a lizardite composition, with only one sample belonging to the chrysotile group[80] (Fig. 3). The presence of chrysotile and lizardite on the plot may suggest serpentinisation, a metamorphic process in which water interacts with minerals, transforming olivine into serpentine minerals. Lizardite, a low-temperature type of serpentine, is stable in relatively colder environments.

The analysis of serpentine phases in all examined rocks indicates chemical signatures consistent with serpentines derived from olivine and orthopyroxene[81] (Fig. 4), suggesting a harzburgitic protolith. Harzburgite is an ultramafic rock typically consisting of olivine and orthopyroxene. The study provides further insights into the original composition of the rocks before modification, as the discovery of a harzburgitic protolith (Fig. 5) reveal their composition before modification[82].

In Figure 6, a triangular diagram classifies trivalent cations in spinel-group minerals found in Serpentinite-Hosted Peridotites (SSPs)[83]. This diagram shows variations in composition based on three trivalent cations: Cr^{3+}, Fe^{3+}, and Al^{3+}. The positions of the plots on the diagram indicate higher levels of Fe within specific fields, suggesting that spinel-group minerals in these areas have a greater proportion of Fe^{3+} than other trivalent cations.

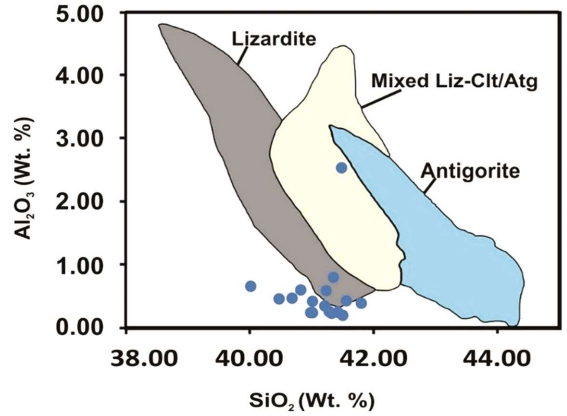

Fig. 3 — Al_2O_3 *vs.* SiO_2 (wt%). Fields of different serpentine minerals after Schwartz *et al.*[80]

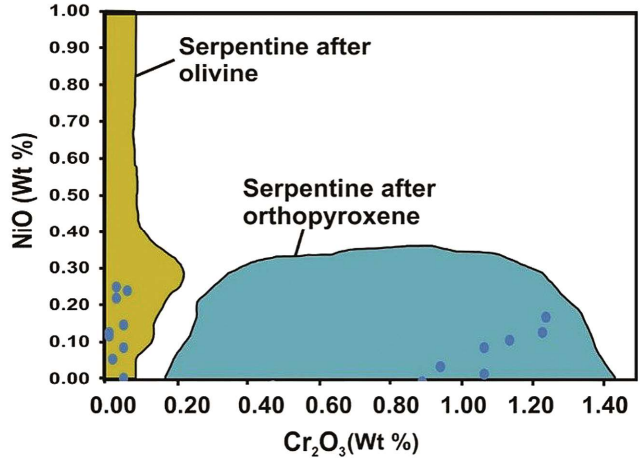

Fig. 4 — NiO *vs.* Cr_2O_3 (wt%). Fields for olivine and orthopyroxene after Kodolánya *et al.*[81]

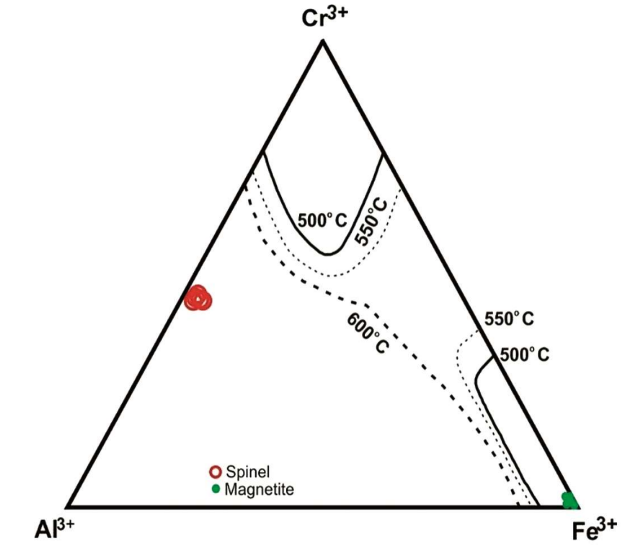

Fig. 5 — A trivalent cation classification triangular diagram, in the context of spinel-group minerals from Serpentinite-Hosted Peridotites (SSPs), is used to illustrate the compositional variations based on three trivalent cations: Cr^{3+}, Fe^{3+}, and Al^{3+}[(ref. 82)]

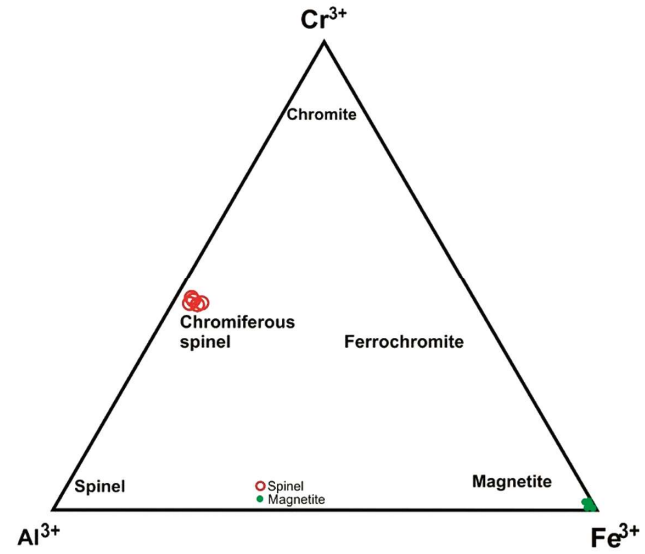

Fig. 6 — Compositional variability in spinel-group minerals from SSPs in a triangular Cr3+– Fe3+ – Al3+ plot[83]

The field of chromiferous spinel[49,83-85] (Fig. 7), which represents spinel minerals containing chromium, is identified within the diagram. The composition of chromiferous spinel, along with its chromium and trace element content, plays a significant role in determining its distinct colours and properties. The observed field of spinel plots falling between Cr and Al suggests that the compositions of spinel-group minerals in serpentinite-hosted peridotites are intermediate between those dominated by Al and Cr compositions.

Spinel is a useful indicator of how much of the Earth's mantle has melted. The chromium number of spinel (Cr#) is an important measure for estimating the extent of partial melting. The composition of chromium-spinel varies, with core chromium numbers (Cr#) ranging from 0.454 to 0.463 (Table S2) and core magnesium numbers (Mg#) ranging from 0.61 to 0.68 (Fig. 8)[86]. Magnetite is mainly found in the groundmass and in the form of veins in the samples being studied (Table S1).

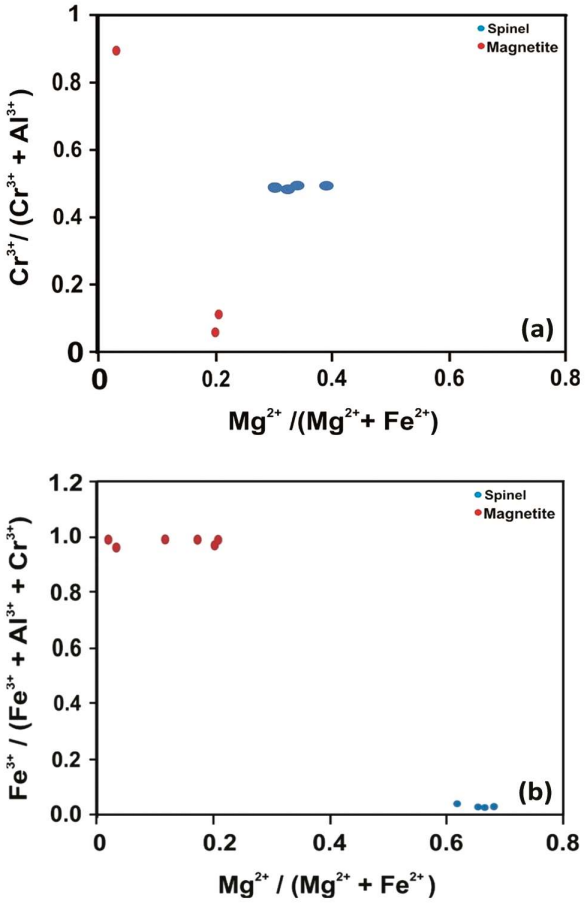

Fig. 7 — Spinel-group mineral compositions from SSPs plotted for $Cr^{3+}/(Cr^{3+}+Fe^{3+})$ against $Mg^{2+}/(Mg^{2+}+Fe^{2+})$[49,83-85]

This finding provides insights into the geological history and petrogenetic processes of peridotites in serpentinite environments. It showcases the compositional diversity and relative proportions of Cr, Fe, and Al in spinel-group minerals.

Trace and REE

The Rock/chondrite *vs*. REE plot (Fig. 9) shows a distinct trend in elements, with a positive peak for Europium (Eu), suggesting the absence of plagioclase feldspar[87]. This trend also indicates enrichment in Light Rare Earth Elements (LREE) and Heavy Rare Earth Elements (HREE) compared to Medium Rare Earth Elements (MREE). A U-shaped pattern in REE from LREE to MREE suggests potential processes

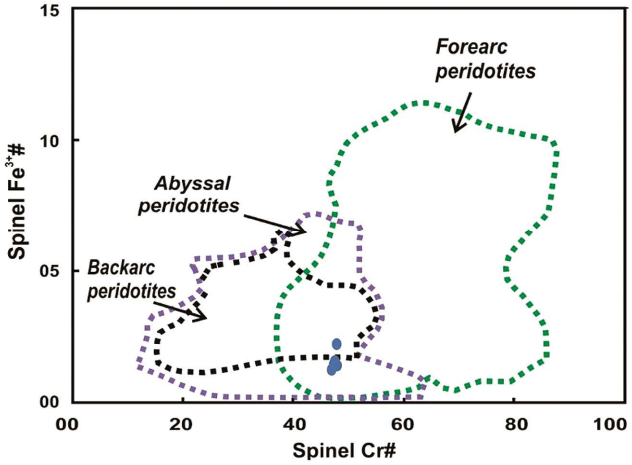

Fig. 8 — Spinel Fe^{3+}# versus Cr#. Fields of forearc, backarc and abyssal peridotites are from Lian *et al*.[86]

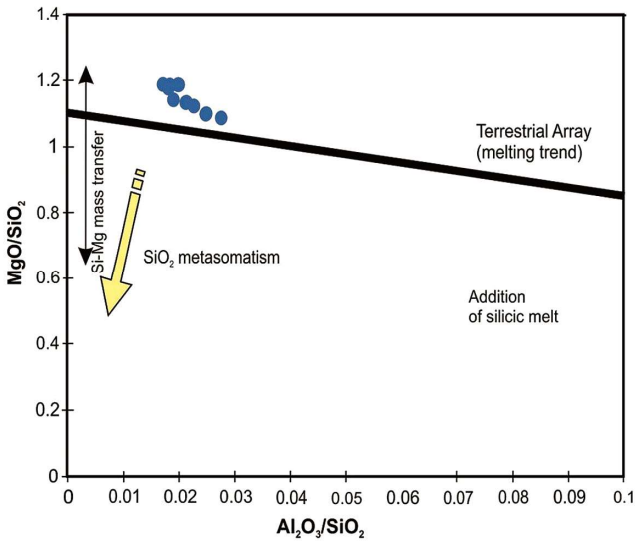

Fig. 9 — Chondrite normalised *vs.* REE plot sowing U shape trend and positive Eu anomaly for serpentinised peridotite. Normalising factors are from Sun & Mc Donough[87]

such as fractional crystallisation. The composition of the initial magma source can influence the distribution of REEs within rocks. REE and trace element data (Fig. 10) reveal various trends and anomalies, including a positive U anomaly, negative Nb anomaly, and positive peaks for Hf, Zr, Eu, Y, and Ho[ref. 87]. Positive U anomalies indicate decreasing conditions during rock formation, while negative Nb anomalies may indicate preferential removal or depletion. Positive peaks for Hf and Zr indicate higher abundance in the rock.

Discussion

Effects of serpentinisation

The investigation of abyssal peridotites has traditionally been hindered by their extensive serpentinisation, which obscures magmatic signatures within their compositions[1,3,5,6,47,49,62,63]. Major-element analyses of bulk-rock abyssal peridotites were not useful for elucidating pre-serpentinisation processes. Niu *et al.*[5-7] employed mineral chemical data and estimated primary mineral modes to reconstruct the bulk-rock compositions of abyssal peridotites prior to serpentinisation building on earlier work by Dick[47]. Quantitative analysis of this data revealed several noteworthy phenomena related to mantle melting and melt extraction processes, sparking debates among researchers[64-69].

In the MgO/SiO_2 *vs.* Al_2O_3/SiO_2 diagram (Fig. 11), the 'terrestrial array' represents progressive magmatic depletion of a primitive mantle, with highly depleted compositions characterised by low Al_2O_3/SiO_2 values[25,70,71]. Upon comparison with the global dataset of abyssal peridotite compiled by Niu[25], it is evident that these samples exhibit a similar trend, albeit systematically offset towards lower MgO/SiO_2 values due to MgO loss during seafloor weathering[24,25]. The observed increase in Al_2O_3/SiO_2 with decreasing MgO/SiO_2 in this dataset can be attributed, at least partially, to melt impregnation within the thermal boundary layer[25]. The global collection of abyssal peridotites examined by Niu[25] shows a trend similar to the terrestrial array reported by Jagoutz *et al.*[70]. This indicates a consistently larger tendency worldwide. The values of Al_2O_3/SiO_2 between 0.1 and 0.3 and those of MgO/SiO_2 between 1 and 1.2–1.4 in CIR samples, fall within typical ranges observed in abyssal peridotites. The absence of Si-Mg mass transfer effects suggests that natural geological processes and environments, such as hydrothermal alteration and mineralogical composition, contributed to the observed geochemical variations.

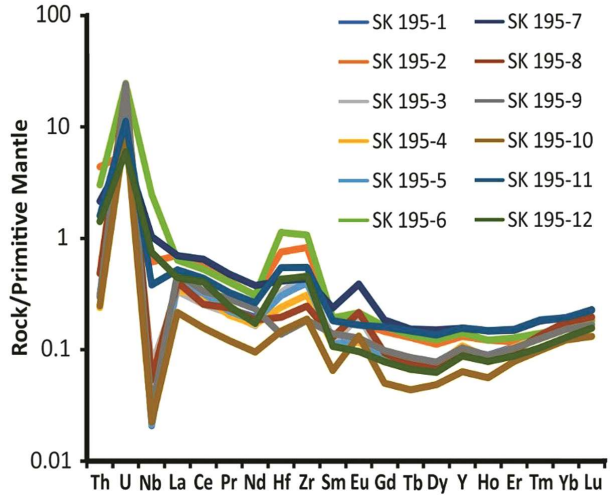

Fig. 10 — Primitive mantle normalised *vs.* REE plot sowing U shape trend and positive Eu anomaly for serpentinised peridotite. Normalising factors are from Sun & Mc Donough[87]

Degree of mantle melting

Lherzolites and harzburgites are common peridotites with varying mineralogical compositions and Mg# ratios. Lherzolites contain magnesium-rich olivine and orthopyroxene, resulting in moderate to high Mg# values. On the other hand, Harzburgites are characterised by their refractory nature, minimal to absent clinopyroxene content, and predominant presence of olivine and orthopyroxene. They often exhibit higher Cr# values due to the absence of clinopyroxene. This results in harzburgites fall within

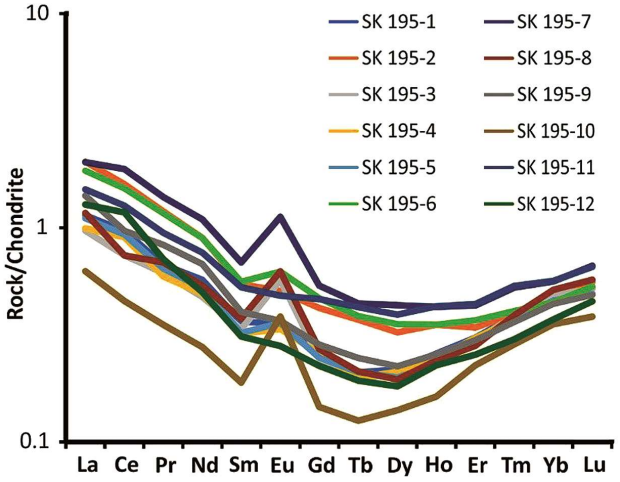

Fig. 11 — MgO/SiO_2 *vs.* Al_2O_3/SiO_2, Data of the abyssal peridotite from the CIR area show a considerable variability whereas analyses of a global set of abyssal peridotite presented by Niu[25] define a trend parallel to the terrestrial array (Jagoutz *et al.*[70])

a field with higher Cr# values, while lherzolites occupy a field with lower Cr# values.

Abyssal peridotites from fast-spreading ridges typically exhibit Cr# values ranging from 0.3 to 0.6, while those from slow-spreading ridges range from 0.1 to 0.3[ref. 72]. Primary spinels in abyssal peridotites generally display low Cr# values, typically ranging from 0.13 to 0.18, with those at the lower end of the abyssal range often associated with lherzolites[73].

The samples from slow-spreading CIR include a range of lherzolite, harzburgite, and abyssal peridotite compositions, as observed from the overlapping fields in the Cr# *vs*. Mg# plot[49] (Fig. 12). The CIR samples exhibit Cr# values ranging from 0.45 to 0.46, placing them within the central to upper range of abyssal peridotites[74,72]. The Cr# value of spinel found in mantle-derived harzburgite and lherzolite indicates the degree of magma extraction[73] during partial melting processes. The average extent of melting calculated for the CIR abyssal harzburgite using Cr# is approximately 16.22 %, aligning with previous studies indicating that the extent of mantle melting ranges around 10 % at the end of a slow-spreading rate and about 22 % at the end of a fast-spreading rate[6].

Hellebrand *et al.*[73] further demonstrated that the melting range for abyssal peridotites extends from approximately 2 % to 18 %. This variation in the extent of melting influences the spreading rates. It underscores the utility of Cr# values for assessing magma-extraction processes in mantle-derived rocks. The rock being abyssal harzburgite was also confirmed by the plots of FeO, Al_2O_3, CaO, SiO_2 *vs*. MgO %[refs. 1,25,49] (Fig. 13).

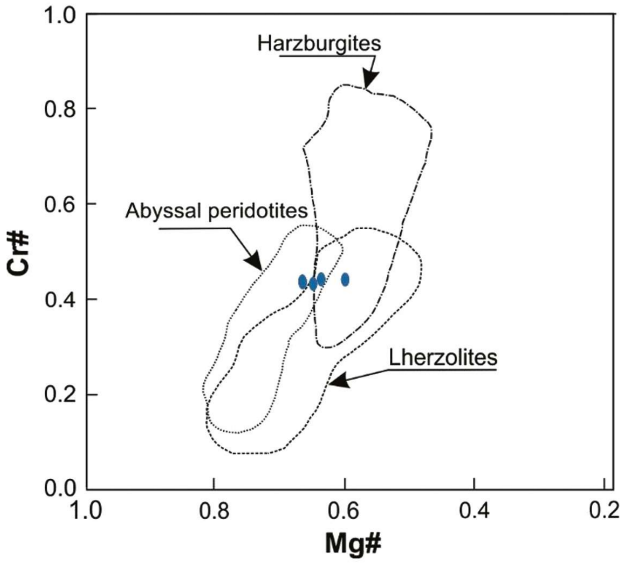

Fig. 12 — Diagram showing the chemical composition of spinels (blue dots) which are plotted in lherzolite, harzbergites and abyssal peridotite fields. The range of spinel from different rocks was concluded by Dick & Bullen[49]

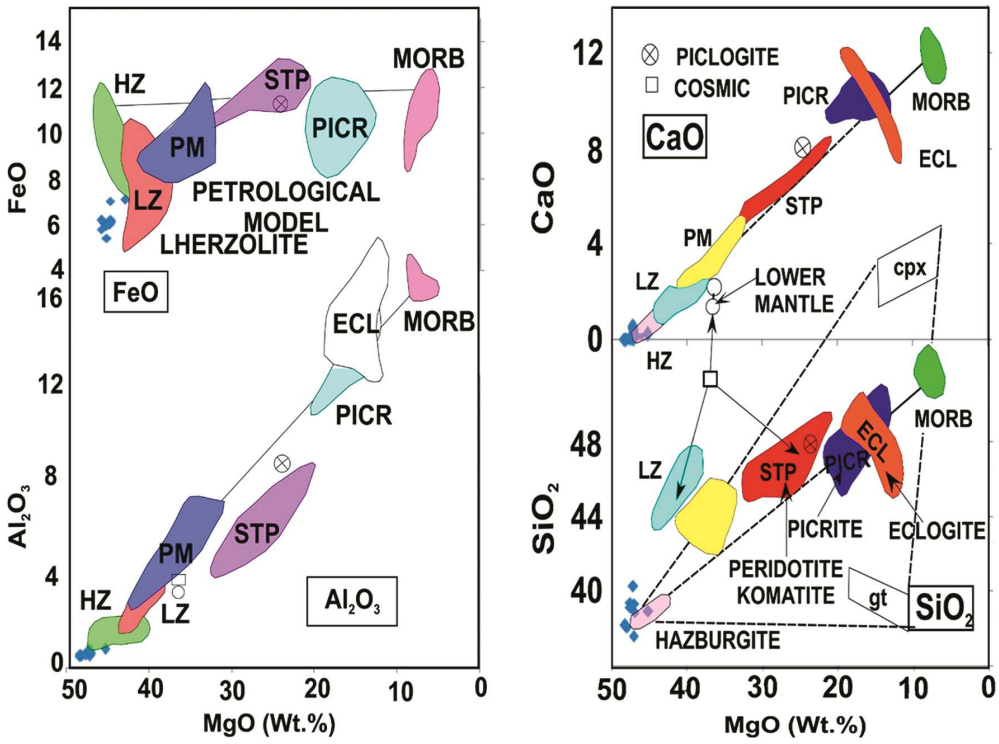

Fig. 13 — Plot of FeO *vs*. MgO, Al_2O_3 *vs*. MgO, SiO_2 *vs*. MgO, and CaO *vs*. MgO, indicative of the type of abyssal peridotite[1,25,49]

While a high Mg# in peridotites suggests minimal crustal interaction, higher Cr# values indicate a wider extent of partial melting in the mantle. The CIR samples fell within the field of Abyssal Peridotites on a partial-melting trend of 15 % (Fig. 14)[49,84].

Serpentinisation, a process in which olivine and pyroxene in peridotite are transformed into serpentine minerals due to hydration, can significantly alter the composition of peridotites. Higher Mg# concentrations in serpentinised peridotites may indicate a more advanced stage of serpentinisation, providing insights into chemical modification and depletion during serpentinisation.

Abyssal peridotites–may represent partially melted mantle rocks. The extent of partial melting can be inferred from the weight % of titanium dioxide (TiO_2), with higher TiO_2 concentrations suggesting greater melting. The TiO_2 *vs*. Cr# plot (Fig. 15) reveals differences in the composition of abyssal peridotites compared to other peridotites, indicating varying degrees of melting or different mantle sources[78,88]. The Cr# ratio, representing chromium concentration relative to the total of aluminium and chromium, is often used as a peridotite geochemical indicator.

Serpentinisation and seafloor weathering cause magnesium loss in peridotites[24,25] , but the inherent magmatic characteristics remain. Robust correlations exist among MgO, Al_2O_3, and CaO due to the preferential depletion of the basaltic component during mantle melting processes[47]. Major composition indicators like Al_2O_3, CaO, MgO/SiO_2, and Al_2O_3/SiO_2 are valuable tools for constraining the extent of mantle peridotite depletion and estimating mantle melting across diverse tectonic regimes, including mid-ocean ridges and subduction zones[5-7,75-77].

The CIR peridotites were juxtaposed with a model of near-fractional mantle melting of major elements[5-7], demonstrating that the correlations among major oxides and the degree of mantle melting are well-preserved despite the loss of MgO.

The Al_2O_3 content in CIR peridotite samples (Fig. 16) is 0–1 %, corresponding to a 25–30 % model melting range[25]. This is expected due to the inverse relationship between MgO and Al_2O_3 concentrations, as aluminium is incorporated into secondary minerals during differentiation processes. Higher MgO concentrations are typically associated with lower Al_2O_3 concentrations, suggesting a negative correlation. The CaO content of the CIR peridotites indicates a partial melting extent exceeding 25%, likely influenced by MgO depletion and CaO reduction due to clinopyroxene alteration[78]. A decrease in CaO concentration is associated with data points clustering around 44–48 weight per cent for MgO and 0–1 % weight per cent for CaO. Lower CaO values correspond to higher MgO values. The model suggests a degree of mantle melting ranging from 6–8% when considering Na_2O concentrations between 0.5–0.7%. This low degree of melting may be

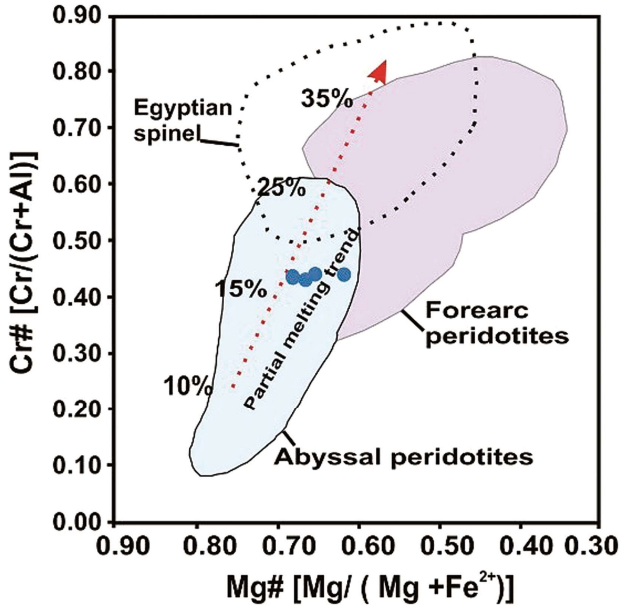

Fig. 14 — Spinel compositions of the studied serpentinite samples plotted on Mg# [Mg/(Mg+Fe^{2+})] *vs*. Cr# [Cr/(Cr+Al)] diagram. Partial melting trend (red arrow) is from Dick & Bullen[49] and Arai[84]

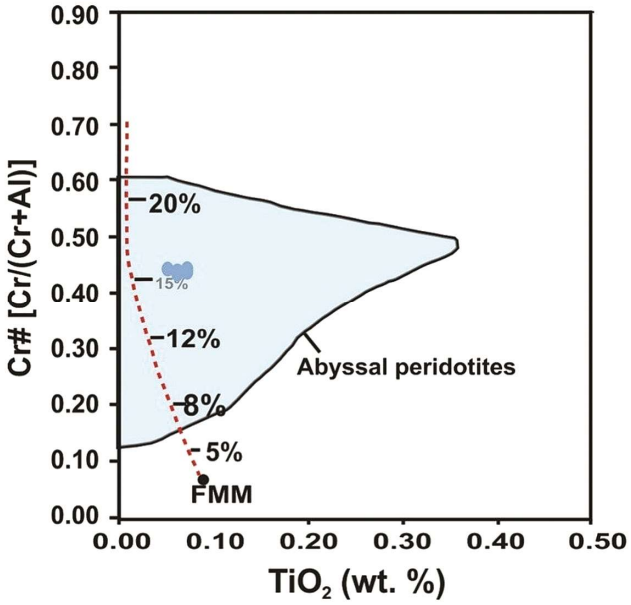

Fig. 15 — Cr# [Cr/(Cr + Al)] *vs*. TiO_2 (wt%). The degrees of melt extractions are from Hellebrand *et al*.[73] and Uysal *et al*.[88]

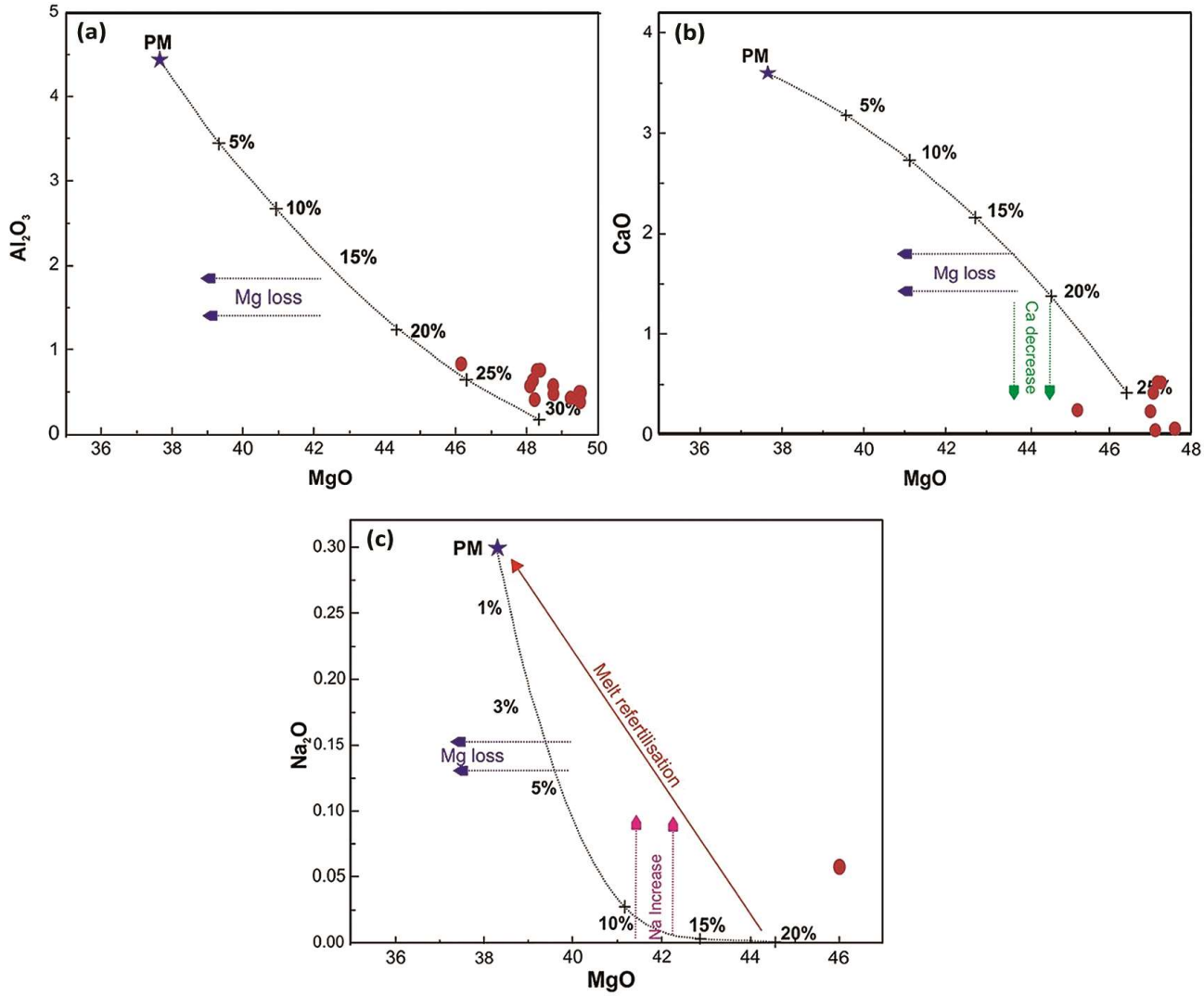

Fig. 16 — Plots of whole-rock MgO contents against a) Al_2O_3; b) CaO; and c) Na_2O (all in wt%). Element concentrations have been recalculated to 100 % on an LOI-free basis. The calculated melting trend for residual serpentinised peridotites using the model of Niu[5] is shown, which assumes anhydrous polybaric near-fractional melting of a PM source from 2.5 GPa to 0.4 GPa. Numbers along the line indicate percentage melting[25]

attributed to Na_2O's heightened susceptibility to mantle heterogeneity and melt fertilisation due to its scarcity in the primitive mantle composition[79] and its high incompatibility during mantle melting processes. Furthermore, Na_2O is susceptible to enhanced melt fertilisation, potentially making it more fertile than the primitive mantle.

The CaO, Al_2O_3, uranium (U), thorium (Th), and zirconium (Zr) concentrations are indicators for estimating mantle melting degrees and understanding geochemical processes[12,25] (Fig. 17). Usually, the concentrations of Zr and Th are inversely proportional. The enrichment in Zr and depletion in Th in CIR rocks may be linked to interactions between serpentinites and immobile trace elements and melts. The variability in thorium concentrations across samples suggests influences from various geological processes, such as differentiation or fractionation.

Melt rock interaction and hydrothermal interaction

The peridotites from the Central Indian Ridge (CIR) exhibit notable compositional heterogeneity, with variations in Rare Earth Element (REE) concentrations attributable to both melt-rock interactions and hydrothermal alteration processes. The behaviour of highly incompatible elements High Field Strength Elements (HFSEs) and REEs is pivotal

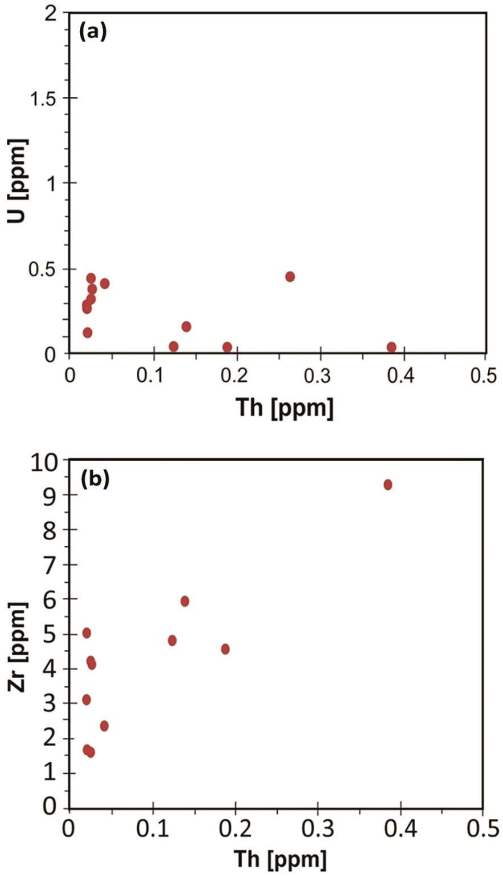

Fig. 17 — Serpentinites from the given study show relatively high immobile trace element concentration indicative for melt-rock interaction processes. a) U *vs*. Th; and (b) Zr *vs.* Th. Symbols as in Figure 3[refs. 12,25]

for understanding their distribution across various geological sites. In aqueous environments, light REEs (LREEs) exhibit greater mobility than heavy REEs (HREEs) and HFSEs. During melt-rock interactions, both LREEs and HFSEs are incorporated into the peridotite in approximately equal proportions.

The positive correlations observed in Nb *vs*. La and Th *vs*. Ce (Fig. 18) indicate that melt-rock interactions are a dominant mechanism driving the observed compositional variations[26,48]. The analysed samples occupy positions in both the melt-rock and fluid-rock interaction fields, indicating the influence of both processes on their geochemical signatures. Nb and La are frequently used as proxies for these interactions due to their distinct geochemical behaviours. The majority of samples cluster within the melt-rock interaction domain, implying that interactions with silicic melts have primarily governed their geochemical composition. Nevertheless, the anomalous distribution in the Nd *vs*. GdN/LuN plot suggests the involvement of additional processes beyond simple melt-rock or fluid-rock interactions that affect the behaviour of these elements.

Tectonic setting

The CIR samples appear to have come from both a supra-subduction zone and abyssal peridotites, suggesting their origin is influenced by multiple tectonic episodes. This study used a geochemical plot showing the concentrations of titanium dioxide and aluminium oxide concentrations in Cr-spinels to analyse their compositions. The unique location of the plot in the supra-subduction zone and abyssal peridotite fields helps differentiate and classify the samples based on their fit into various tectonic contexts. The Al_2O_3 *vs*. TiO_2 binary plot (Fig. 19) helps understand the petrogenetic processes, mineralogical compositions, and tectonic histories of the samples[85].

Alpine peridotites can provide insights into the mantle source, the extent of melting, and interactions with other crustal materials during ascent. The study of alpine peridotites was conducted using the trivalent cations triangle diagram, commonly used to assess Cr-spinels in peridotites hosted by serpentinite. The triangle plot (Fig. 20) includes three trivalent cations: $Cr^{3}+$, $Fe^{3}+ + 2Ti^{4}+$, and $Al^{3}+$[ref. 89]. Selecting trivalent cations is crucial in understanding the compositional changes of Cr-spinels in peridotites hosted by serpentinite. The data points/plots lie within the field linked to alpine peridotites, indicating that the Cr-spinel compositions in these peridotites align with the geochemical signature characteristic of alpine peridotites.

The Fe-Cr-Al ternary plot, encompassing fields such as Nidar peridotites, Mariana forearc peridotites, and abyssal peridotites, reveals that the spinel samples predominantly plot within the abyssal peridotite field (Fig. 21)[49]. This positioning confirms that the rock type is characteristic of abyssal peridotite settings. The ternary plot effectively illustrates the mineralogical composition based on the concentrations of iron, chromium, and aluminium. The highlighted fields of Nidar peridotites, abyssal peridotites, and Mariana forearc peridotites delineate distinct geochemical domains. The spinel samples, located within the abyssal peridotite field, exhibit a geochemical signature akin to that of abyssal peridotites, implying a common geological origin or mechanism. These samples likely originated from

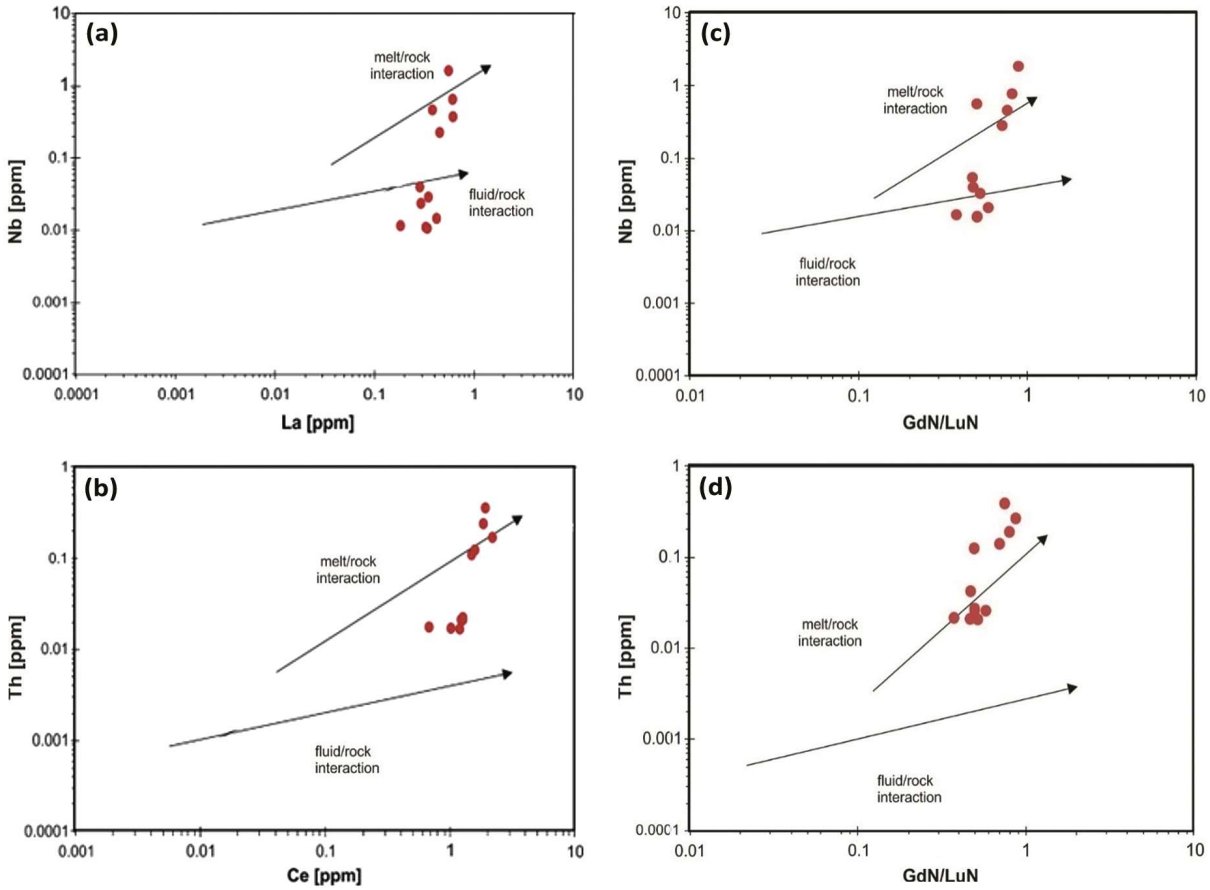

Fig. 18 — Deviating trends for melt-rock interaction and hydrothermal alteration: a) Nb *vs*. La; b) Th *vs.* Ce; c) Nd *vs*. Gd/LuN; and d) Th *vs*. Gd/LuN[refs. 26,48]

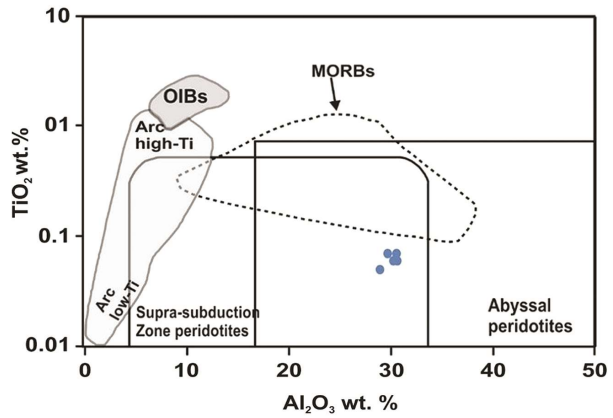

Fig. 19 — Al_2O_3 *vs*. TiO_2 binary plot (after Kamenetsky *et al*.[85]) of Cr-spinels in comparison to modern-day tectonic settings

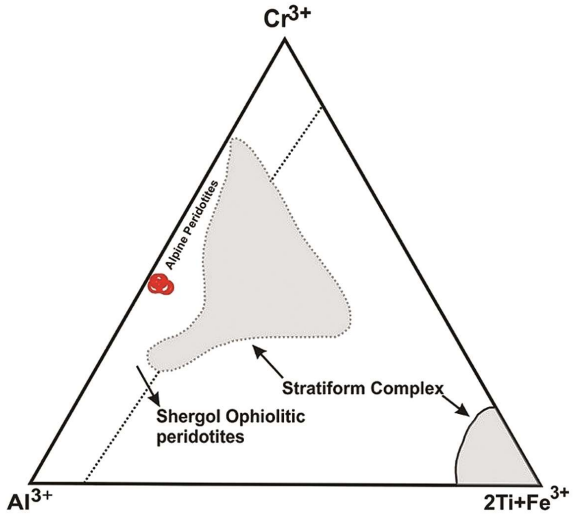

Fig. 20 — Triangular trivalent cation plot of Al^{3+}– (Fe^{3+}+2Ti^{4+}) Cr^{3+} (after Jan & Windley[89]) for Cr-spinels from SSPs

abyssal plains or oceanic spreading centres, reflecting similar geological environments. The geochemical congruence suggests a shared source material or mantle reservoir, with analogous tectonic and magmatic processes influencing the formation of these peridotites. The occurrence of the samples in the abyssal peridotite region may indicate partial melting or magma differentiation, potentially linked to igneous events.

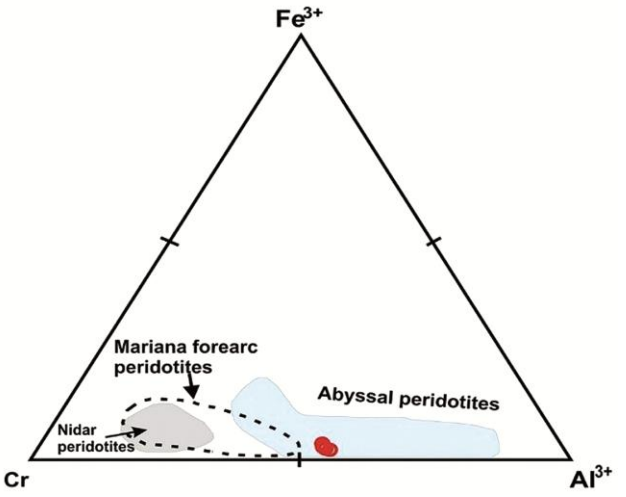

Fig. 21 — Ternary plot of Fe-Cr-Al showing fields such as nidar peridotites, mariana forearc peridotites, abyssal peridotites, wherein the spinel samples are plotting in the field of abyssal peridotites[49]

Conclusion

Petrographic analysis of serpentinised peridotite has delineated its mineralogical composition, confirming the presence of olivine, pyroxene, spinel, magnetite, and serpentine polymorphs. The high degree of serpentinisation was evidenced by the presence of antigorite, various serpentine polymorphs, inclusions, alteration veins, mesh textures, and brucite formation. Major oxide analysis identified an atypical negative magnesium trend, suggesting differentiation processes in olivine-serpentine transformations, distinct from typical seafloor weathering patterns. Trace and rare earth element analysis indicated that negative Nb anomalies result from magma extraction in subduction zones, while positive Hf and Zr anomalies suggest crystal melting and magma differentiation.

The Cr# *vs*. TiO_2 and Mg# plots confirmed the serpentinised peridotites as abyssal harzburgites associated with ocean ridges. Further, derived partial-melting values suggest these rocks originated from a mantle source, experiencing significant melting. Mineral classification and tectonic setting analysis predominantly classify these rocks as abyssal peridotites setting, with indications of alpine peridotite and supra-subduction zones. The Cr-spinel characteristics reinforce an abyssal peridotite origin, indicating a common geological mechanism.

Supplementary Data

Supplementary data associated with this article is available in the electronic form at https://nopr.niscpr.res.in/jinfo/ijms/IJMS_54(08)398-413_SupplData.pdf

Acknowledgments

The authors are deeply grateful to the School of Earth, Ocean and Atmospheric Sciences (SEOAS), Goa University, for their constant encouragement and for providing the necessary academic resources. The authors further acknowledge CSIR–National Institute of Oceanography, Goa, for granting permission and extending valuable assistance, which were essential for the completion of this research.

Conflict of Interest

The Authors declare that there is no conflict of interests.

Author Contributions

MP: Writing - original draft preparation, methodology, data analysis and data curation; PDS: Data analysis and data curation, conceptualisation, investigation, supervision; and RM: Field work, sample collection, supervision, and editing.

References

1 Dick H J, Fisher R L & Bryan W B, Mineralogic variability of the uppermost mantle along mid-oceanic ridges, *Earth Planet Sci Lett*, 69 (1) (1984) 88-10.

2 Cannat M, Mevel C, Maia M, Deplus C, Durand C, *et al.*, Thin crust, ultramafic exposures, and rugged faulting patterns at the Mid-Atlantic Ridge (22-24 N), *Geology*, 23 (1) (1995) 49-52.

3 Johnson K T, Dick H J & Shimizu N, Melting in the oceanic upper mantle: an ion microprobe study of diopsides in abyssal peridotites, *J Geophys Res: Solid Earth*, 95 (B3) (1990) 2661-2678.

4 Elthon D, Chemical trends in abyssal peridotites: refertilization of depleted suboceanic mantle, *J Geophys Res: Solid Earth*, 97 (B6) (1992) 9015-9025.

5 Niu Y, Mantle melting and melt extraction processes beneath ocean ridges: evidence from abyssal peridotites, *J Petrol*, 38 (8) (1997) 1047-1074.

6 Niu Y & Henkinian R, Spreading-rate dependence of the extent of mantle melting beneath ocean ridges, *Nature*, 385 (6614) (1997) 326-329.

7 Niu Y, Languir C H & Kinzler R J, The origin of abyssal peridotites: a new perspective, *Earth Planet Sci Lett*, 152 (1-4) (1997) 251-265.

8 Hellebrand E, Snow J E & Muhe R, Mantle melting beneath Gakkel Ridge (Arctic Ocean): abyssal peridotite spinel compositions, *Chem Geol*, 182 (2-4) (2002) 227-235.

9 Brunelli D, Seyler M, Cipriani A, Otoolini L & Bonatti E, Discontinuous melt extraction and weak refertilization of mantle peridotites at the Vema lithosphere section (Mid-Atlantic Ridge), *J Petrol*, 47 (4) (2006) 745-771.

10 Seyler M, Lorand J P, Dick H J & Drounin M, Pervasive melt percolation reactions in ultra-depleted refractory harzburgites at the Mid-Atlantic Ridge, 15 20' N: ODP Hole 1274A, *Contrib Mineral Petrol*, 153 (2007) 303-319.

11 Tamura A, Arai S, Ishimaru S & Andal E S, Petrology and geochemistry of peridotites from the Mid-Atlantic Ridge and implications for mantle melting processes, *Contrib Mineral Petrol*, 155 (2008) 491–509.

12 Godard M, Lagabrielle Y, Alard O & Harvey J, Geochemistry of highly depleted peridotites drilled at ODP sites 1272 and 1274 (Fifteen-Twenty Fracture Zone, Mid-Atlantic Ridge): Implications for mantle dynamics beneath a slow spreading ridge, *Earth Planet Sci Lett*, 267 (3-4) (2008) 410-425.

13 Macdonald A H & Fyfe W S, Rate of serpentinisation of seafloor environments, *Tectonophysics*, 116 (1-2) (1985) 123-135.

14 Ferry J M, Contrasting mechanisms of fluid flow through adjacent stratigraphic units during regional metamorphism, south- central Maine, USA, *Contrib Mineral Petrol*, 98 (1) (1988) 1-12.

15 Dick H J, Lin J & Schouten H, An ultra slow-spreading class of ocean ridge, *Nature*, 426 (6965) (2003) 405-412.

16 Sauter D, Carton H, Mendel V, Munschy M, Rommevaux-Jestin C, *et al*., Ridge segmentation and the magnetic structure of the Southwest Indian Ridge (at 50 degree 30' E, 55 degree 30' E and 66 degree 20' E): Implications for magmatic processes at ultraslow-spreading centres, *Geochem Geophys Geosys*, 5 (5) (2004) p. Q05004.

17 Cochran J K, Landman N H, Turekian K K, Michard A & Schrag D P, Paleoceanography of the late Cretaceous (Maastrichtian) Western Interior seaway of North America: evidence from Sr and O isotopes, *Palaeogeogr Palaeoclimatol Palaeoecol*, 191 (1) (2003) 45-64.

18 Lagabrielle Y, Cannat M & Briais A, Formation of oceanic core complexes by detachment faulting and magmatism at slow-spreading ridges, *Geology*, 26 (8) (1998) 711-714.

19 Escartin J, Hirth G & Evans B, Effects of serpentinization on the lithospheric strength and the style of normal faulting at slow-spreading ridges, *Earth Planet Sci Lett*, 151 (3–4) (1997) 181–189.

20 Escartín J, Hirth G & Evans B, Strength of slightly serpentinized peridotites: Implications for the tectonics of oceanic lithosphere, *Geology*, 29 (2001) 1023–1026.

21 Hirose K, Karato S I, Cormier V F, Brodholt J P & Yuen D A, Unsolved problems in the lowermost mantle, *Geophys Res Lett*, 33 (12) (2006) 1-4, Art No L12S01.

22 Hirose K, Kawamura K, Ohishi Y, Tateno S & Sata N, Stability and equation of state of $MgSiO_3$ perovskite to the core–mantle boundary, *Geophys Res Lett*, 33 (1) (2006) Art No L01310.

23 Hilairet N, Reynard B, Wang Y, Daniel I, Merkel S, *et al*., High-pressure creep of serpentine, interseismic deformation, and initiation of subduction, *Science*, 318 (5858) (2008) 1910–1913.

24 Snow J E & Dick H J, Pervasive magnesium loss by marine weathering of peridotite, *Geochim Cosmochim Acta*, 59 (20) (1995) 4219–4235.

25 Niu Y, Bulk-rock major and trace element compositions of abyssal peridotites: implications for mantle melting, melt extraction and post-melting processes beneath mid-ocean ridges, *J Petrol*, 45 (12) (2004) 2423–2458.

26 Paulick H, Bach W, Godard M, Hoog J, Suhr G, *et al*., Geochemistry of abyssal peridotites (Mid-Atlantic Ridge, 15°20′ N, ODP Leg 209): implications for fluid/rock interaction in slow-spreading environments, *Chem Geol*, 234 (2006) 179–210.

27 Kelley D S, Karson J A, Fruh-Green G L, Yoerger D R, Shank T M, *et al*., A serpentinite-hosted ecosystem: the Lost City hydrothermal field, *Science*, 307 (5714) (2005) 1428–1434.

28 Takai K, Nakagawa S, Reysenbach A L & Hoek J, Microbial ecology of mid-ocean ridges and back-arc basins, In: *Back-Arc Spreading Systems: Geological, Biological, Chemical, and Physical Interactions*, Geophysical Monograph Series, Vol 166, edited by Christie D M, Fisher C R, Lee S-M & Givens S, (American Geophysical Union), 2006, pp. 185–213.

29 Morishita T, Hara K, Nakamura K, Sawaguchi T, Tamura A, *et al*., Igneous, alteration and exhumation processes recorded in abyssal peridotites and related fault rocks from an oceanic core complex along the Central Indian Ridge, *J Petrol*, 50 (2009) 1299–1325.

30 Karson J A, Thompson G, Humphris S E, Edmond J M, Bryan W B, *et al*., Along-axis variations in seafloor spreading in the MARK area, *Nature*, 328 (6132) (1987) 681–685.

31 Bienvenu P, Bougault H, Joron J L, Treuil M & Dmitriev L, MORB alteration: rare-earth element/non-rare-earth hygromagmaphile element fractionation, *Chem Geol*, 82 (1990) 1–14.

32 Cannat M, Bideau D & Bougault H, Serpentinized peridotites and gabbros in the Mid-Atlantic Ridge axial valley at 15°37′ N and 16°52′ N, *Earth Planet Sci Lett*, 109 (1–2) (1992) 87–106.

33 Cannat M & Casey J F, An ultramafic lift at the Mid-Atlantic Ridge: successive stages of magmatism in serpentinized peridotites from the 15°N region, In: *Mantle and Lower Crust Exposed in Oceanic Ridges and in Ophiolites*, (Springer, Dordrecht), 1995, pp. 5–34.

34 Bideau D, Hébert R, Hekinian R & Cannat M, Petrology of ultramafic rocks from the Mid-Atlantic Ridge, *J Geophys Res*, 101 (1996) 13615–13634.

35 Escartín J, Mével C, MacLeod C J & McCaig A M, Constraints on deformation conditions and the origin of oceanic detachments: the Mid-Atlantic Ridge core complex at 15°45′ N, *Geochem Geophys Geosyst*, 4 (8) (2003) 1-37.

36 Escartin J, Smith D K & Cannat M, Parallel bands of seismicity at the Mid-Atlantic Ridge, 12–14° N, *Geophys Res Lett*, 30 (12) (2003) 1-4.

37 Bach W, Garrido C J, Paulick H, Harvey J & Rosner M, Seawater–peridotite interactions: first insights from ODP Leg 209, MAR 15° N, *Geochem Geophys Geosyst*, 5 (9) (2004) 1-22.

38 Hébert R, Bideau D & Hekinian R, Ultramafic and mafic rocks from the Garrett transform fault near 13°30′ S on the East Pacific Rise: igneous petrology, *Earth Planet Sci Lett*, 65 (1) (1983) 107–125.

39 Iyer S D & Ray D, Structure, tectonics and petrology of mid-oceanic ridges and the Indian scenario, *Curr Sci*, 85 (3) (2003) 277–289.

40 Hamlyn P R & Bonatti E, Petrology of mantle-derived ultramafics from the Owen Fracture Zone, *Earth Planet Sci Lett*, 48 (1) (1980) 65–79.

41 Engel C G & Fisher R L, Granitic to ultramafic rock complexes of the Indian Ocean ridge system, western Indian Ocean, *Geol Soc Am Bull*, 86 (11) (1975) 1553–1578.

42 Bassias Y & Triboulet C, Petrology and P-T-t evolution of the South West Indian Ridge peridotites. A case study: east of the Melville Fracture zone at 62°E, *Lithos*, 28 (1) (1992) 1–19.

43 Seyler P T & Boaventura G R, Distribution and partition of trace metals in the Amazon basin, *Hydrol Process*, 17 (7) (2003) 1345–1361.

44 Arai S, Characterization of spinel peridotites by olivine–spinel compositional relationships: review and interpretation, *Chem Geol*, 113 (3–4) (1994) 191–204.

45 Ross K & Elthon D, Cumulus and postcumulus crystallization in the oceanic crust, In: *Proc Ocean Drilling Program Sci Results*, NSF, 1997, pp. 333–350.

46 Ross K & Elthon D, Extreme incompatible trace-element depletion of diopside in residual mantle, In: *Proc Ocean Drilling Program Sci Results*, NSF, 1997, pp. 277–284.

47 Dick H J B, Abyssal peridotites, very slow spreading ridges and ocean ridge magmatism, *Geol Soc Lond Spec Publ*, 42 (1989) 71–105.

48 Bach W, Paulick H, Garrido C J, Ildefonse B, Meurer W P, *et al.*, Unraveling the sequence of serpentinization reactions, *Geophys Res Lett*, 33 (13) (2006) Art No L13306.

49 Dick H J & Bullen T, Chromian spinel as a petrogenetic indicator, *Contrib Mineral Petrol*, 86 (1984) 54–76.

50 Mahoney J J, Natland J H, White W M, Poreda R, Bloomer S H, *et al*., Isotopic and geochemical provinces of western Indian Ocean spreading centers, *J Geophys Res Solid Earth*, 94 (B4) (1989) 4033–4052.

51 Natland J, Indian ocean crust, In: *Oceanic Basalts*, (Springer, Boston), 1991, pp. 289–310.

52 Natland J, Mineralogy and crystallization of oceanic basalts, In: *Oceanic Basalts*, (Springer, Boston), 1991, pp. 63–93.

53 Rehka M & Hofmann A W, Recycled ocean crust and sediment in Indian Ocean MORB, *Earth Planet Sci Lett*, 147 (1–4) (1997) 93–106.

54 Ray R, Sheth H C & Mallik J, Structure and emplacement of the Nandurbar–Dhule mafic dyke swarm, *Bull Volcanol*, 69 (2007) 537–551.

55 Ray D, Misra S, Banerjee R & Weis D, Geochemical implications of gabbro from the slow-spreading ridge, *Geol Mag*, 148 (3) (2011) 404–422.

56 Ray J S, Kumar A, Sudheer A K, Deshpande R D, Rao D K, *et al*., Origin of gases and water in mud volcanoes, *Chem Geol*, 347 (2013) 102–113.

57 Ray M C, Hilton D R, Muñoz J, Fischer T P & Shaw A M, Volatile recycling and degassing, *Chem Geol*, 266 (1–2) (2009) 38–49.

58 Charlou J L & Donval J P, Hydrothermal methane venting, *J Geophys Res Solid Earth*, 98 (B6) (1993) 9625–9642.

59 Edmonds H N, Michael P J, Baker E T, Connelly D P, Snow J E, *et al*., Hydrothermal venting on Gakkel Ridge, *Nature*, 421 (2003) 252–256.

60 Bach W, Banerjee N R, Dick H J & Baker E T, Discovery of ancient and active hydrothermal systems along the ultra-slow spreading Southwest Indian Ridge 10°–16° E, *Geochem Geophys Geosyst*, 3 (7) (2002) 1-15.

61 Kiselev E A, Chemical composition of serpentine minerals, *Geol Ore Deposits*, 60 (6) (2018) 452–468.

62 Michael P J & Bonatti E, Peridotite composition from North Atlantic, *Earth Planet Sci Lett*, 73 (1) (1985) 91–104.

63 Johnson K T & Dick H J, Open system melting at Atlantis II fracture zone, *J Geophys Res Solid Earth*, 97 (B6) (1992) 9219–9241.

64 Asimow P D, Model for abyssal peridotites, *Earth Planet Sci Lett*, 169 (3–4) (1999) 303–319.

65 Baker M B & Beckett J R, Origin of abyssal peridotites, *Earth Planet Sci Lett*, 171 (1) (1999) 49–61.

66 Niu Y, Collerson K D, Batiza R, Wendt J I & Regelous M, Origin of enriched MORB, *J Geophys Res Solid Earth*, 104 (B4) (1999) 7067–7087.

67 Niu Y & O'Hara M J, Origin of ocean island basalts: A new perspective from petrology, geochemistry, and mineral physics considerations, *J Geophys Res Solid Earth*, 108 (B4) (2003) 1-19.

68 Walter M J, Melting residues and melt extraction in the upper mantle, *Earth Planet Sci Lett*, 169 (1999) 337–350.

69 Lundstrom C C, Gill J & Williams Q, MORB generation hypothesis, *Chem Geol*, 162 (2) (2000) 105–126.

70 Jagoutz E, Palme H, Baddenhausen H, Blum H, Cendales M, *et al*., The abundances of major, minor and trace elements in the earth's mantle as derived from primitive ultramafic nodules, In: *Proc 10th Lunar Planet Sci Conf*, 1979, pp. 2031–2050.

71 Hart S R & Zindler A, Bulk Earth composition, *Chem Geol*, 57 (3–4) (1986) 247–267.

72 Lee Y I, Detrital chromian spinel review, *Geosci J*, 3 (1999) 23–29.

73 Hellebrand E, Snow J E, Dick H J & Hofmann A W, Coupled major and trace elements, *Nature*, 410 (2001) 677–681.

74 Hamdy M M & Lebda E M, Chromitites variation, *J Geol Min Res*, 3 (9) (2011) 232–250.

75 Takazawa E, Frey F A, Shimizu N & Obata M, Horoman peridotite, *Geochim Cosmochim Acta*, 64 (4) (2000) 695–716.

76 Takazawa E, Okayasu T & Satoh K, Geochemistry and origin of the basal lherzolites from the northern Oman ophiolite (northern Fizh block), *Geochem Geophys Geosyst*, 4 (2) (2003) 1-31.

77 Barth M G, Mason P R D, Davies G R & Drury M R, Othris ophiolite, *Lithos*, 100 (2008) 234–254.

78 Ulrich M, Picard C, Guillot S, Chauvel C, Cluzel D, *et al*., New Caledonia ophiolite, *Lithos*, 115 (1–4) (2010) 223–236.

79 Workman R K & Hart S R, Depleted MORB mantle, *Earth Planet Sci Lett*, 231 (1–2) (2005) 53–72.

80 Schwartz S, Guillot S, Reynard B, Lafay R, Debret B, *et al.*, Pressure–temperature estimates of the lizardite/antigorite transition in high-pressure serpentinites, *Lithos*, 178 (2013) 197–210.

81 Kodolányi J, Pettke T, Spandler C, Kamber B S & Gméling K, Geochemistry of ocean floor and fore-arc serpentinites: Constraints on the ultramafic input to subduction zones, *J Petrol*, 53 (2) (2012) 235–270.

82 Irvine T N, Chromian spinel as a petrogenetic indicator. Part 2. Petrologic applications, *Can J Earth Sci*, 2 (6) (1965) 648–672.

83 Barnes S J & Roeder P L, The range of spinel compositions in terrestrial mafic and ultramafic rocks, *J Petrol*, 42 (12) (2001) 2279–2302.

84 Arai S, Chemistry of chromian spinel in volcanic rocks as a potential guide to magma chemistry, *Mineral Mag*, 56 (383) (1992) 173–184.

85 Kamenetsky V S, Crawford A J & Meffre S, Factors controlling chemistry of magmatic spinel: An empirical study of associated olivine, Cr-spinel and melt inclusions from primitive rocks, *J Petrol*, 42 (4) (2001) 655–671.

86 Lian D, Yang J, Dilek Y & Rocholl A, Mineralogy and geochemistry of peridotites and chromitites in the Aladağ Ophiolite (southern Turkey): Melt evolution of the Cretaceous Neo-Tethyan mantle, *J Geol Soc (Lond)*, 176 (5) (2019) 906–925.

87 Sun S S & McDonough W F, Chemical and isotopic systematics of oceanic basalts: Implications for mantle composition and processes, In: *Magmatism in the Ocean Basins*, edited by A D Saunders & M J Norry, Geological Society, London, Special Publications, 42 (1989) 313–345.

88 Uysal İ, Ersoy E Y, Karslı O, Sadıklar M B, Ottley C J, *et al.*, Coexistence of abyssal and ultra-depleted SSZ-type mantle peridotites in a Neo-Tethyan ophiolite in SW Turkey: Constraints from mineral composition, whole-rock geochemistry (major–trace elements and PGE) and Re–Os isotope systematics, *Lithos*, 132–133 (2012) 50–69.

89 Jan M Q & Windley B F, Chromian spinel-silicate chemistry in ultramafic rocks of the Jijal Complex, northwest Pakistan, *J Petrol*, 31 (3) (1990) 667–715